



Research Article

Green synthesis of zinc oxide nanoparticles and zinc oxide–silver, zinc oxide–copper nanocomposites using *Bridelia ferruginea* as biotemplate

E. Gurgur¹  · S. S. Oluyamo² · A. O. Adetuyi¹ · O. I. Omotunde³ · A. E. Okoronkwo¹

Received: 28 November 2019 / Accepted: 17 February 2020 / Published online: 16 April 2020
© Springer Nature Switzerland AG 2020

Abstract

The quest to synthesize nanomaterials with improved properties, but less undesirable effects on the environment necessitated this research. Zinc Oxide (ZnO) nanoparticles and zinc oxide–silver (ZnO–Ag), zinc oxide–copper (ZnO–Cu) nanocomposites were synthesized with pure eco-friendly dye extracted from *Bridelia ferruginea*, zinc acetate ($\text{Zn}(\text{CH}_3\text{COO})_2$) as host, copper acetate ($\text{Cu}(\text{CH}_3\text{COO})_2$), and silver nitrate (AgNO_3) as dopant precursors. Phytochemical screening of dyes showed high, presence of phenols and terpenoids. The nanomaterials were characterized by Fourier-transform infrared, X-ray diffraction, scanning electron microscopy with energy dispersive X-ray analysis, transmission electron microscopy and ultraviolet–visible spectroscopy. The results showed the capping agents in the dyes were responsible for reducing the bulk materials. The crystallinity of the nanomaterials were found to be 19.02, 18.98 and 18.90 nm for the ZnO, ZnO–Ag and ZnO–Cu nanoparticles respectively. The ZnO nanoparticles were flakelike in shape, whereas the Cu and Ag doped particles were spherical. An optical bandgap of 4.73 eV was recorded for the dye and 3.24 eV for the ZnO nanoparticles. This was narrowed to 3.18 and 3.13 eV by silver and copper dopant respectively. These results showed the nanoparticles as a potential agent for photovoltaics and other optical applications.

Keywords *Bridelia ferruginea* · Green synthesis · Nanoparticles · Nanocomposites · Dye

1 Introduction

Nanoscience and nanotechnology are divest fields that modify bulk materials and improve their optical, electronic, magnetic, and catalytic properties [1], these properties are targeted at improving human lives. As global warming has ravaged the universe, the world scientists are trying hard to open new doors to finding novel technologies in the development of new materials with unique characteristics [2] but of low environmental hazard. The known two types of nanomaterials are the organic and inorganic nanoparticles. The former being poly- ϵ -lysine, quaternary ammonium compounds, cationic quaternary polyelectrolytes,

and Chitosan. The latter being mainly oxides of silver (Ag), iron (Fe), titanium (Ti), copper (Cu), zinc (Zn) and other transition element. The stability of the inorganic particles at variable temperature gave it a wide range of industrial applications [3, 4]. Metallic nanoparticles are synthesized by different techniques; the more frequently employed methods are the chemical and physical methods. Several chemical methods had been identified, but researchers work more on chemical reduction, electrochemical techniques, and photochemical reactions in synthesizing and modifying nanomaterials [1, 3, 5]. The attrition and pyrolysis techniques took center stage under physical method, although the technique is brand as wasteful due to its

✉ E. Gurgur, tgurgur24@gmail.com | ¹Department of Chemistry, The Federal University of Technology, Akure, Ondo, Nigeria. ²Department of Physics, The Federal University of Technology, Akure, Ondo, Nigeria. ³Department of Chemistry Education, The Federal University, Oye, Ekiti, Nigeria.



high cost, high-energy consumption and low output rate [3, 6]. The consciousness of environmental deterioration has cautioned scientists to look towards greener approach which is an inexpensive nontoxic approach in synthesizing and fabricating nanomaterials [1]. Recently extracts of unicellular organisms, as well as plants have recorded tremendous success in the synthesis of nanoparticles of different shapes and sizes [7]. However, synthesis of nanomaterials using microorganisms is arduous because of the complex and complicated nature of isolating, maintaining cell cultures and multiple purification steps. Hence, it is advisable to synthesize nanoparticles using plant materials due to their availability and the procedure of biogenic synthesis is cost efficient, less tedious as compared to biosynthesis using fungal sources [8]. Several metal oxide nanoparticles had been produced with possible industrial applications. Among these, ZnO is the most exploited at nano-dimensions because of its exceptional scientific properties attributed to its band gap and large excitonic binding energy [9]. It has become a focal point of nowadays research considering its tremendous antimicrobial activity against a wide range of microorganisms. *S. aureus*, *E. coli*, Salmonella, Listeria monocytogenes, and the fungus Fusarium [10, 11]. Doping ZnO nanoparticles with Copper, Cobalt, Nickel, rare earth metals, and transition elements, as impurities modified the nanoparticles to enhance their electrical, optical and biological activities [12–14]. Silver and Copper doped ZnO nanoparticles have gained great interest in growing a full scope of innovative applications including field effect transistors, field emission arrays, ultraviolet lasers, light emitting diode, sensors, biosensors, catalyst, energy storage and solar cell [15, 16].

In recent times nanomaterials are synthesized with templates which are perceived easy with simplified procedures to give room for better fabrication of more sophisticated nanomaterials [17]. Templates are categorized into two groups of soft and hard. Porous solids like anodic aluminium oxide (AAO) membranes, colloid beads, ordered mesoporous inorganic materials, and zeolites are regarded as hard templates. Soft templates are organic molecules, long-chain polymers, supermolecular aggregates, structure-directing agents, surfactants, gels, micelles, and different types of biological species (biotemplates). Soft templates did not only render more sufficient synthetic processes, but also have the ability to be easily removed, these have proven their effectiveness and shown their ability in high quality encapsulation techniques [18, 19]. Dyes were believed to be substances that only impact colour to textiles, sequel to the dominance of synthetic dyes. But with the arrival of natural dyes, their benefits and values have been appreciated in all areas of life, especially in natural medicine, food and recently nanotechnology [20]. Natural dyes are usually not a single entity, but a variety

of closely related chemical compounds, which enhance their therapeutic roles in natural medicine, impact colour to fabrics, reduce and cap ions in nanoscience. The complex chemical constituents in natural dyes are Anthraquinones, Naphthoquinones, Benzoquinones, Flavonoids, Carotenoids and Tannins [21]. Synthesis of nanoparticles by solvent extracted dyes from *B. ferruginea* is sparingly reported, implying the plant is underexploited on nanodimension. This motivated our interest in this research. Our focus is to extract dyes from *B. ferruginea* that belongs to the family Euphorbiaceae and found mostly in Savannah regions. It has dark grey, rough and oftentimes marked scaly bark [22]. The plant is a major actor in traditional medicine; with its extract playing a significant role in the formulation of a traditional gargle “egun efu” and water treatment [23]. A handful of reports on the bark extract has proven its high anti-typanocidal, anti-molluscidal, antimicrobial and anti-inflammatory properties [24]. The leaves also demonstrated curative effect towards the treatment of diabetes and as a purgative. [25, 26]. The curative strength of *B. ferruginea* has been attributed to its high antioxidants and phytochemicals, hence it can serve as an excellent agent in the reduction of $\text{Zn}(\text{CH}_3\text{COO})_2$, $\text{Cu}(\text{CH}_3\text{COO})_2$ and AgNO_3 to their nanoparticles and nanocomposites, as well as capped the ions to their states.

2 Materials and methods

2.1 Chemicals

The following chemicals $\text{Zn}(\text{CH}_3\text{COO})_2$, $\text{Cu}(\text{CH}_3\text{COO})_2$, AgNO_3 , n-hexane and methanol were obtained from Sigma-Aldrich and used without further purification. All solutions were prepared with deionize water.

2.2 Sample collection and preparation

The bark of *Bridelia ferruginea* used as the source of the dye was collected from a farmland at Ido Usi, Ekiti State of Nigeria, Sun dried, ground, sieved to have uniformed particles and were stored in an airtight container for the extraction of the dye.

2.3 Extraction of dye

Soxhlet apparatus was used for the extraction of dyes. The Pulverized sample was loaded in the thimble and mounted on the round bottom flask. The sample was first defatted with n-Hexane for 6 h at a heating rate of 68 °C. The defatted samples were offloaded from the thimble, sundried to remove the trapped n-hexane and reloaded for the dyes

extraction using methanol at the heating rate of 65 °C. The dyes were oven dried at 40 °C to powder.

2.4 Green synthesis of nanoparticles and nanocomposites

The nanoparticles were synthesized using green synthesis method as reported by Yedurkar et al, [27], with the exclusion of NaOH that acted as a pH stabilizing agent. 10 g of the dye was dissolved in 100 ml of methanol, filtered with Whatman filter paper to remove any undissolved particles. 50 ml of the dye's filtrate was added 100 ml (0.5 M) of $Zn(CH_3COO)_2$ was allowed to stand for 2 h at room temperature. The initial light brown colouration of the solution became a deep brown crowded solution indicating the complete formation of the precipitate. This affirmed the reduction of zinc acetate to zinc oxide nanoparticles. The mixture was stirred for 1 h, centrifuged for 30 min and

washed severally with deionized water and ethanol. The pure reduced ZnO nanoparticles were oven dried at 80 °C for 6 h and calcined at 500 °C for 1 h. The nanocomposites were synthesized by mixing 100 ml (0.5 M) of $Zn(CH_3COO)_2$ with 100 ml (0.05 M) of $AgNO_3$ or $Cu(CH_3COO)_2$ for the synthesis of ZnO–Ag and ZnO–Cu respectively. The solution was stirred for 2 min on a magnetic stirrer and the methanolic extract of the dye was added to the mixture. The finishing protocol for ZnO was adopted for the composites. Figure 1 presents a schematic representation of the synthetic pathway for the particles (Scheme 1).

2.4.1 Reaction mechanism for the synthesis of ZnO nanoparticle and ZnO–Ag nanocomposite

The presence of tannins, terpenoid and flavonoids in the dye extract which behave as ligands and their special ability to chelate various metal ions enhance the reduction

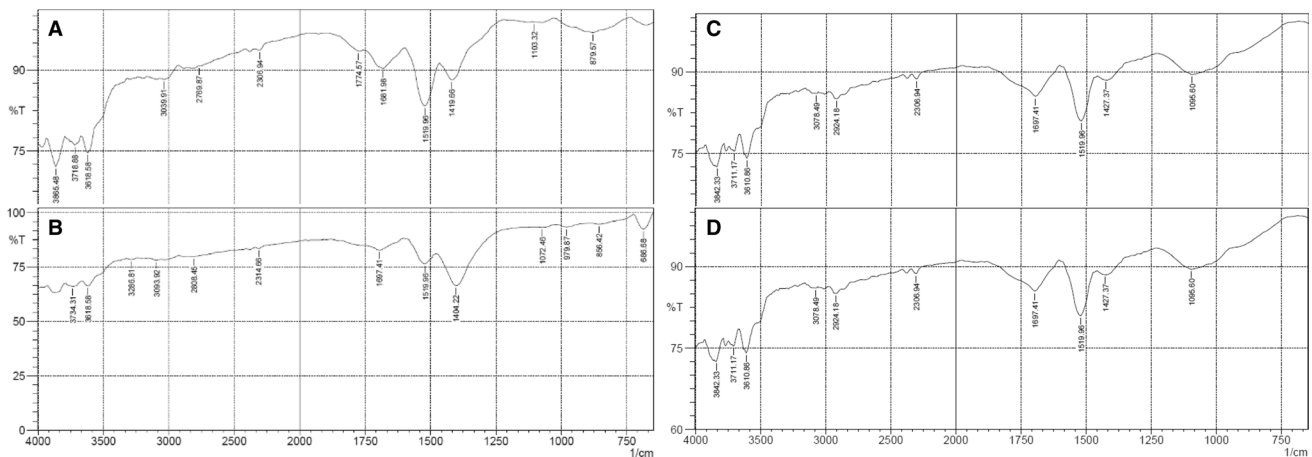
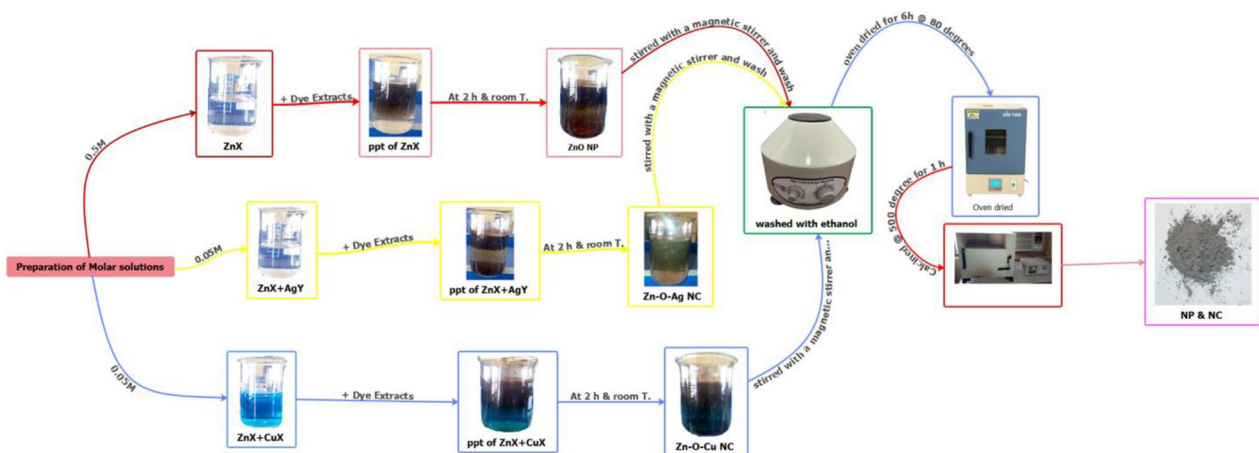
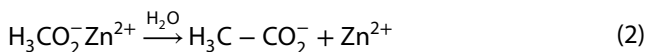
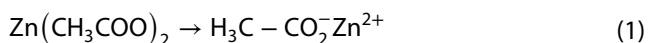


Fig. 1 FTIR of a ZnO Nanoparticle b ZnO–Ag Nanocomposite c ZnO–Cu Nanocomposite d dye of *B. ferruginea*



Scheme 1 Schematic representation of the synthetic pathway of ZnO nanoparticles (NP) and ZnO–Ag and ZnO–Cu nanocomposite

and subsequent stabilization of the ions to their nano form. Among the phytochemical constituents, flavonoids readily chelate metal ions and create complex compounds due to their ability to donate electrons and hydrogen atoms. Zinc acetate, Copper acetate and silver trioxonitrate (V) dissolved in water to become freely moving ions as shown in the Eqs. (1 and 2) for Zinc acetate.



The free ions attack the active sites on the phenolic compound present in the dye extract to gain stability hence, reducing it to its nano form. The large number of "OH" functional groups in phytochemical is a major factor in the reduction process. This factor favours the formation of a hydrophilic surfaces arising from the dissolved oxygen (from air) molecules, that are suitable for the growth of nanoparticles [28]. The Mechanism pathway for the synthesis of ZnO–Ag nanocomposite is the same as ZnO–Cu nanocomposite synthesis (Scheme 2).

2.5 Phytochemical analysis of the dye

Phytochemical screening was performed on the dye to ascertain the presence of reducing and capping agent present in the dye extracts. The assays to investigate are; tannins, steroids, phlobatannins, saponins, flavonoids, phenols, anthocyanins and terpenoids and using established methods [30–32, 33].

2.5.1 Test for tannin

10 ml of bromine water was added to the 0.5 g aqueous extract. Decoloration of bromine water confirmed the presence of tannins

2.5.2 Test for steroids

2 ml of chloroform and concentrated H₂SO₄ were added with the 5 ml aqueous plant crude extract. In the lower chloroform layer red color appeared that indicated the presence of steroids

2.5.3 Test for phlobatannin

1% aqueous HCl acid was added to 5 ml of the extract, it was then boiled with the help of Hot plate stirrer. The absence of a red precipitate was evidence for the absent of phlobatannins in this sample.

2.5.4 Test for saponins

5.0 ml of distilled water was vigorously mixed with aqueous crude plant extract in a test tube. Few drops of olive oil was added to the mixture upon froth appearance and vigorously mixed. The appearance of foam confirmed the presence of saponins.

2.5.5 Test for flavonoids

Alkaline Reagent Test were used to confirm the presence of flavonoids in bark of *B. ferruginea*. 2 ml of 2.0% NaOH mixture was mixed with crude aqueous extract of the plant; concentrated yellow color was produced, which became colorless when 2 drops of diluted acid was added to the mixture. This result showed the presence of flavonoids.

2.5.6 Test for phenol

5 ml of the methanolic plant extract was mixed with 2 ml of 2% FeCl₃ solution. A blue-green or black coloration indicated the presence of phenols

2.5.7 Test for cyanogenic glycoside

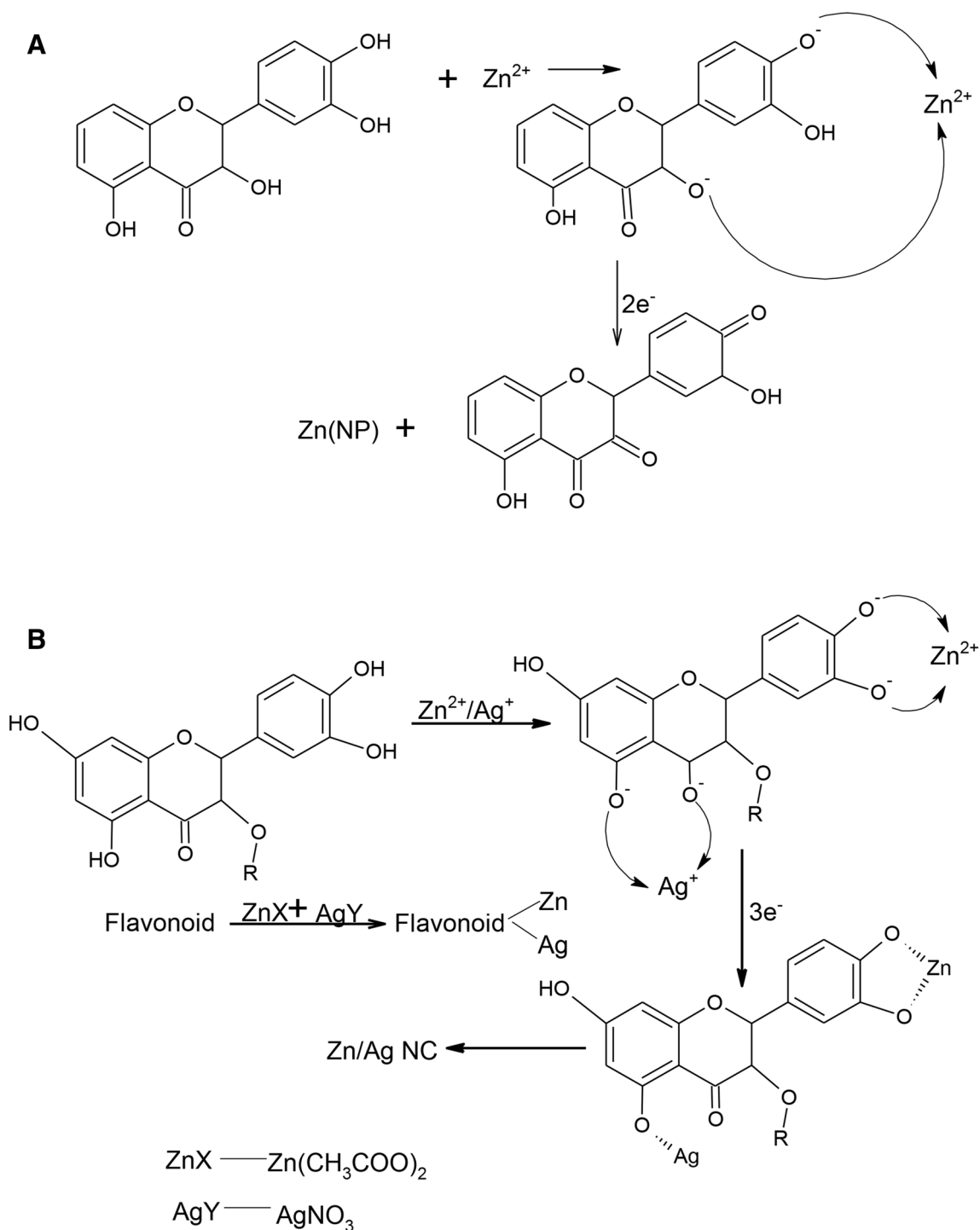
Sodium picrate test or Guignard reaction was used to confirm the presence of anthocyanins. A soaked filter paper strips was first in 10% picric acid and then in 10% sodium carbonate and dried. The extracts were taken in small bottles and the strips were suspended from the mouth of the container and the lids were tightly closed with portion of the strip stuck in the lid. The strips did not turn brick red nor maroon indicating the absence of cyanogenic glycosides (anthocyanins)

2.5.8 Test for terpenoids

Chloroform (2 ml) was added to aqueous plant extract (5 ml) and evaporated on a water bath and then boiled with 3 ml of concentrated H₂SO₄. A grey coloration attests to the presence of terpenoids.

2.6 Characterization of biosynthesized ZnO nanoparticles and ZnO nanocomposite of Silver or Copper

The FTIR (Shimadzu Co. Ltd., Kyoto, Japan) was used with KBr pellets in the wavelength range 4000–500 cm⁻¹ for identification of the functional groups involved in the reduction of the precursors to nanoparticles and nanocomposites. The phase formation, purity and crystallinity of the nanoparticles were recorded using XRD (GBC eMMA). The visual properties of ZnO nanoparticles



Scheme 2 Schematic mechanism for the synthesis of **a** ZnO Nanoparticles and **b** ZnO–Ag nanocomposite (Idea from work of Ahmad et al. [29] and Mohammed et al. [28])

and nanocomposites were investigated, based on UV–Vis absorption spectra in the wavelength range of 200–800 nm. The morphologies, elemental composition

and particle size were investigated using SEM equipped with an EDX (Quanta 200—FEI coupled to EDS probe) and TEM (TECNAI G2 SPIRIT-FEI).

3 Results and discussion

3.1 Phytochemical analysis

The methanolic dye extract was screened for major phytochemicals as shown in Table 1. Aside the biological and the therapeutic properties, the metabolites are reported to have excellent reducing and stabilizing ability towards the reduction of bulk metals to the nano forms [34]. High extract yields of phenols and terpenoids were recorded in the dye. This is ascribed to the high polarity of methanol solvent to a variety of plant constituents [31]. The presence of these molecules gives the dyes the expected self-assembly and ability to cap the metal nanoparticles formed, thereby inducing controlled morphology [35].

Among the metabolites, terpenoids and phenols isolated from plants are implicated in successfully catalyzing the reduction of bulk material to nano ions [30, 34]. The ability of phenol to act as capping agent lies in the presence of hydroxyl and carboxylic group which makes it a good chelator [36], impacting it with ability to stabilize metal ions [37]. The presence of the two metabolites gave the dye the expected strength to reduce bulk materials and stabilize the metal ions. The absence of anthocyanine confirmed report in literatures that, it can only exist in storage tissues of the plants [38].

3.2 FTIR spectroscopy of the synthesized nanoparticles and nanocomposites

FTIR (Fig. 1) was used to identify the possible functional groups that are actively involved in the reduction of $\text{Zn}(\text{CH}_3\text{COO})_2$, AgNO_3 and $\text{Cu}(\text{CH}_3\text{COO})_2$ to various nanoparticles and nanocomposite. A broad peak at 3394.83 cm^{-1} for *B. ferruginea* dyes is assigned hydrogen O–H band stretching, but shifted to 3618.58 cm^{-1} on the spectra of ZnO nanoparticles, ZnO–Ag and ZnO–Cu nanocomposites [39]. The dyes have a crest at 1635.69 cm^{-1}

which is characteristic of aldehydes C=O stretches, but slightly moved to higher frequencies on the spectra of ZnO nanoparticles, ZnO–Ag and ZnO–Cu nanocomposite. A H–C–H asymmetric and symmetric stretch peak was found at 2931 cm^{-1} on the dye's spectrum, but at 2924.18 cm^{-1} for ZnO–Cu and 2808.92 cm^{-1} for ZnO–Ag nanocomposites. The peak at 1527 cm^{-1} on the dye spectra is for N–H bends. This however appears as N–H stretching at 3286 cm^{-1} for ZnO–Ag. The spectral bands at 1419.66 cm^{-1} , 1427.37 cm^{-1} and 1450.52 cm^{-1} confirmed the presence of C–H bending, while 1103.32 cm^{-1} , 1072.46 cm^{-1} , 1095.60 cm^{-1} correspond to C–O stretching for ZnO, ZnO–Ag, ZnO–Cu respectively. The crest at 1411.94 cm^{-1} on the FTIR spectra of the dyes is typical of S=O stretching, but this appeared on a lowered frequency of 1404.22 cm^{-1} on ZnO–Ag nanocomposite. The functional groups between 686.68 and 879.57 cm^{-1} correlates to metal oxide bands [5].

The absence of S=O, N–H bends, H–C–H asymmetric and symmetric bands on the spectra of ZnO nanoparticles and ZnO–Cu nanocomposite spectra confirmed that the functional groups were used up in the reduction of the zinc acetate and Copper acetate [40]. All the band and functional groups identified are peculiar to the phytoconstituents identified in the phytochemical screening [41].

3.3 UV–visible spectroscopy

Figure 2 presents the UV–Vis absorption spectra of ZnO nanoparticles, ZnO–Ag and ZnO–Cu nanocomposites and the dye. There is an excitonic peak between 206 nm for the dyes and 251 nm for the ZnO–Ag, these peaks are characteristic of the polyphenolic compounds which acted actively during the synthetic and reduction processes between the phyto-compounds of *B. ferruginea*, and metal precursors [42]. These peaks also pointed to presence of ZnO nanoparticles, which lies much below the bandgap wavelength [41]. Peaks between 300 and 400 nm are characteristic of ZnO nanoparticles which may be due to the electron transition from the valence band to the conduction band. The appearance of distinctive peaks of low absorption intensity on the spectra of ZnO nanoparticles, ZnO–Ag and ZnO–Cu nanocomposite between 320 and 360 nm confirmed the formation of ZnO nanoparticles [43]. The reduction in the peak intensity in the spectra of the ZnO–Ag and ZnO–Cu indicated the inclusion of Ag^{2+} and Cu^{2+} in the matrix of the nanocomposites and suggested some level of agglomeration with irregular shapes [44]. The region of absorption of the spectrum suggested the suitability of the nanomaterials for both UV and visible region [45].

Table 1 Phytochemical constituents of *Bridelia ferruginea*

Phytochemical test	Absent	present	Slightly present	Heavily present
Tannin			++	
Steroids			++	
Phlobatainins		+		
Sapoinis		+		
Flavonoids		+		
Phenols				+++
Anthocyanins	–			
Terpenoids				+++

Fig. 2 UV-Vis Absorption spectroscopy of ZnO nanoparticles, ZnO–Ag nanocomposite, ZnO–Cu nanoparticles and dyes

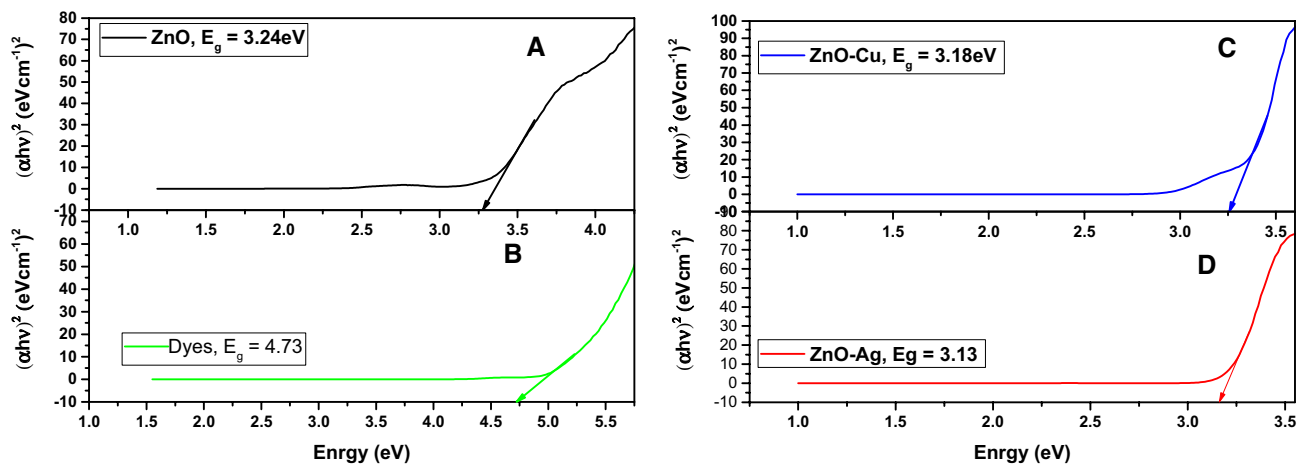
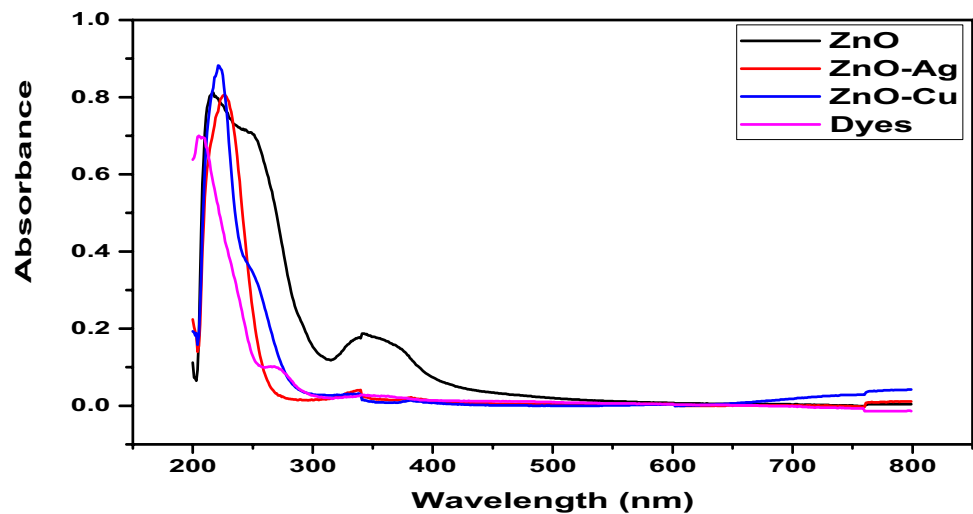


Fig. 3 Tauc's plot for optical band gap of **a** ZnO nanoparticles, **b** dyes, **c** ZnO–Cu nanocomposite and **d** ZnO–Ag nanocomposite

The optical band gap (Fig. 3), was estimated using Tauc's plot for direct transition semiconductor, by extrapolating the straight line of $(\alpha h\nu)^2$ versus $h\nu$ graph. High band gap energy of 4.73 eV is recorded for the dye, but was reduced to 3.24 eV in ZnO nanoparticles. The introduction of Ag and Cu impurities in the nanocomposite narrowed the band gap to 3.18 eV and 3.12 eV for ZnO–Cu and ZnO–Ag respectively.

This narrowing of band gap became prominent as Zn^{2+} is gradually substituted by Cu^{2+} and Ag^{2+} in the matrix of the materials and systematically increased the number of oxygen vacancies due to their ion radii and electronegativity [46]. More so, the impurities created a special defect, which simulates the Fermi level to rise towards the conduction [41, 45, 47, 48]

Figure 4 is the XRD diffractogram of ZnO nanoparticle, ZnO–Ag and ZnO–Cu nanocomposites. The peaks at

2θ of 31.62° , 34.30° , 36.11° , 47.41° , 56.47° , 62.75° , 67.83° and 68.95° for ZnO nanoparticles diffractogram lie in the crystallographic planes of (100), (001), (101), (102), (110), (103), (112) and (201). These agree with standard JCPDS card No. 89-0510, and correspond to the Hexagonal wurtzite [42, 49–51]. The crystallography of ZnO–Ag showed peaks that correspond to 2θ values 26.84° , 29.46° , 31.95° , 44.96° , 47.42° , 50.89° , 53.33° , 56.28° , 63.45° and 68.82° and within the crystallographic planes of (111), (111), (200), (220), (220), (311), (222), (311), (400) and (331). These are concordant with JCPDS No. 89-4937. The peaks at 26.84° , 29.46° and 31.95° are due to the presence of bio-organic phases on the surface of the particles [44], these would have been contributed by the polyphenolic compounds. Characteristic peaks of Ag^+ signal appeared at 2θ 4.96° and 63.45° . This attest to the presence of Ag^+ in the ZnO–Ag nanocomposite. A similar diffractogram was reported by

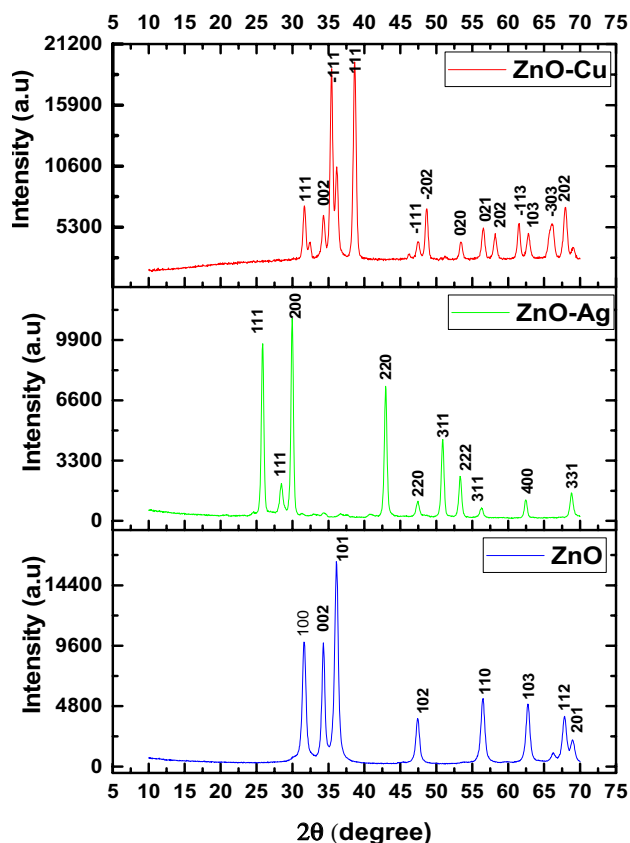


Fig. 4 The X-ray Diffraction of **a** ZnO nanoparticle **b** ZnO–Ag and **c** ZnO–Cu nanocomposite

Dinesha et al., when he dope ZnO with Ag [52]. However, there is an overlap of Ag^+ signals with the wurtzite plane at (311), (400) and (331). The influence of doped Ag onto ZnO significantly altered the peak orientation, due to replacement of Ag^+ into host ZnO crystal lattice [53]. All the other peaks confirmed in the XRD graph of ZnO–Ag nanocomposite are assigned to ZnO nanoparticles. The diffractograms of ZnO–Cu nanoparticles show peaks in the crystallographic plan of (002) and (101) which are typical of ZnO nanoparticles. The crystallographic peaks of 2θ at 35.55° , 38.65° , 47.47° , 48.66° lies in the plane of $(-1\ 1\ 1)$, $(1\ 1\ 1)$, $(-2\ 0\ 2)$. These are in consonance with the XRD pattern, with the presence of copper doped on the ZnO [3]. There is an overlapping of the Cu and Zn signals, especially at a 2θ value of 62.81° , 66.02° and 67.95° . The extra peaks are plant phytoconstituents which probably escaped the washing of ZnO–Ag during the synthesis.

The Highly absorbed diffraction peaks confirmed the significant crystallinity of ZnO, ZnO–Ag and ZnO–Cu nanomaterials. The unavailability of other diffracted peaks on the diffractogram of ZnO and ZnO–Ag authenticates the high purity of the synthesized ZnO nanoparticles [7, 41]. The decrease in peak's intensity on the ZnO–Ag and

ZnO–Cu diffractograms, is a behavioural pattern peculiar to decreased crystallite sizes in the presence of the dopant. There is a slight shift on the ZnO peaks accounting for the present AgO and CuO fused in the ZnO wurtzite lattice. The secondary phase of AgO and CuO diffraction peaks indicated the formation of AgO–ZnO and CuO–ZnO nanocomposite. The change in the crystallite size and a shift on ZnO on the diffractogram is the confirmation of the presence of Ag and Cu incorporated into the Zn site [3, 17, 54].

The average grain size of the sample, was calculated using the Debye Scherer's equation

$$D = \frac{0.9\lambda}{\beta \cos \theta} \quad (3)$$

where D is Crystal size (nm), is the wavelength of the XRD used, is FWHM, and is Bragg's angle [40, 45, 55]. X-ray diffractogram was analyzed to obtain information about various crystalline aspects of ZnO nanoparticle, ZnO–Ag and ZnO–Cu nanocomposite materials. The average crystallite size of ZnO, ZnO–Ag and ZnO–Cu is about 19.02 nm, 18.98 and 18.90 nm respectively.

3.4 SEM and EDX analysis of ZnO nanoparticles, ZnO–Ag and ZnO–Cu nanocomposites

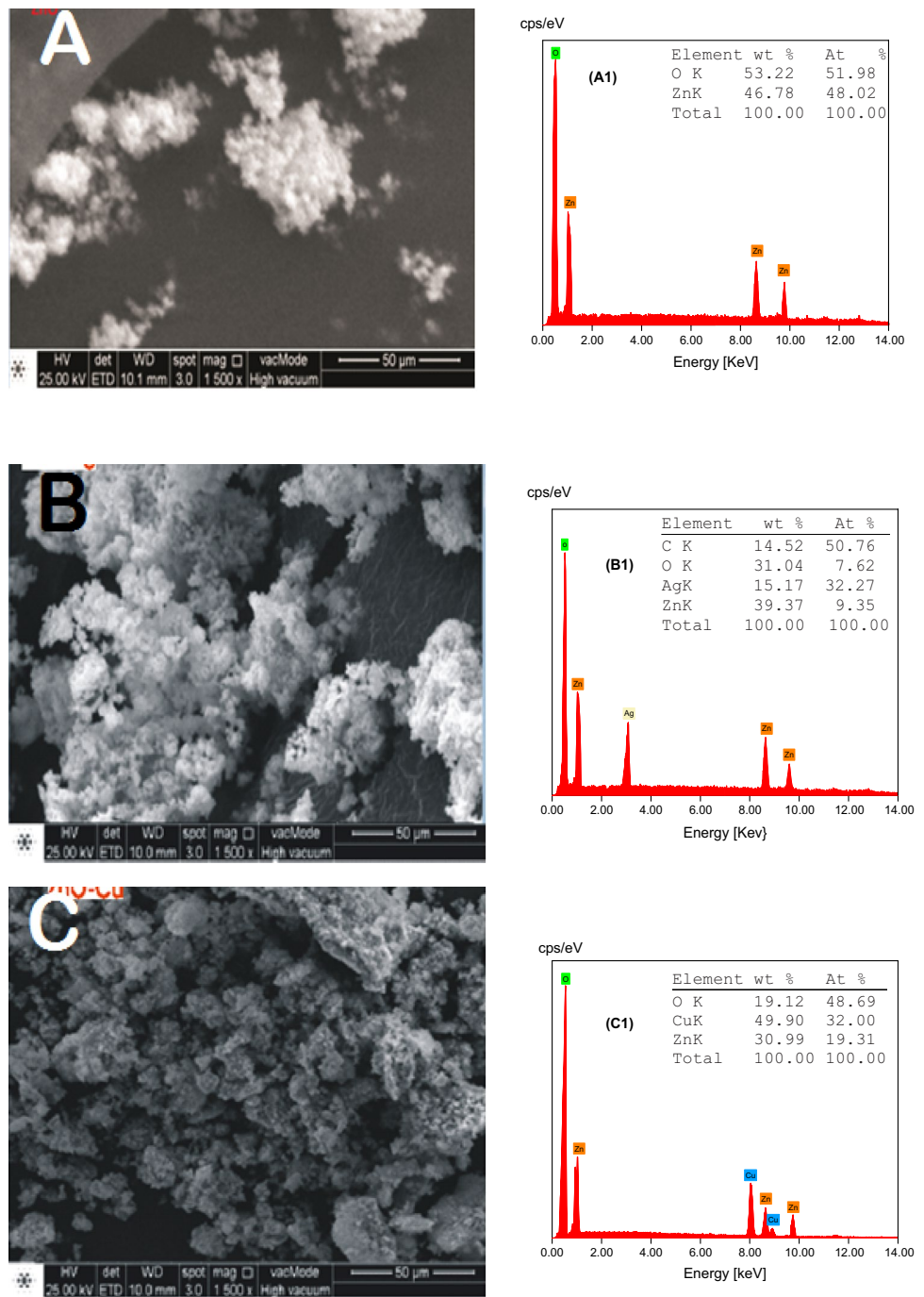
The morphological feature and the elemental composition of the nanomaterials synthesised were investigated using SEM equipped with an EDX as shown in Fig. 5. The SEM picture of ZnO nanoparticles confirmed the formation of nanoparticles with approximate nodular like shape. There was no significant change in the morphology upon the addition of Ag dopant but with the addition of Cu impurities, the nodular like shape aggregated into larger particles with pores but no well-defined morphology. This aggregation may be due to the presence of secondary metabolites in the leaf extracts [39] as confirmed by the XRD. The presence of Zn, O, Ag and Cu were confirmed by EDX Fig. 5(a1–c1).

A strong peak for O appeared at about 0.5 keV with Zn^{2+} ion on 1.08 keV, 8.59 keV and 9.82 keV. Ag^{2+} is at 3.09 keV and Cu^{2+} peak appeared on binding energy 8.1 keV. A strong signal of O on the EDXs of the synthesized nanomaterials, is partly contributed by X-ray emission from the phytochemicals of the dye.

3.5 TEM and SAED pattern of the materials

The TEM images in Fig. 6 give detailed structural analysis of the synthesized materials. The image (Fig. 6a) shows the presence of nanorods coexisting with nanoflakes in ZnO nanoparticles. Image of ZnO–Ag in Fig. 6b revealed a polyhedral shape of ZnO with Ag dots on the surface

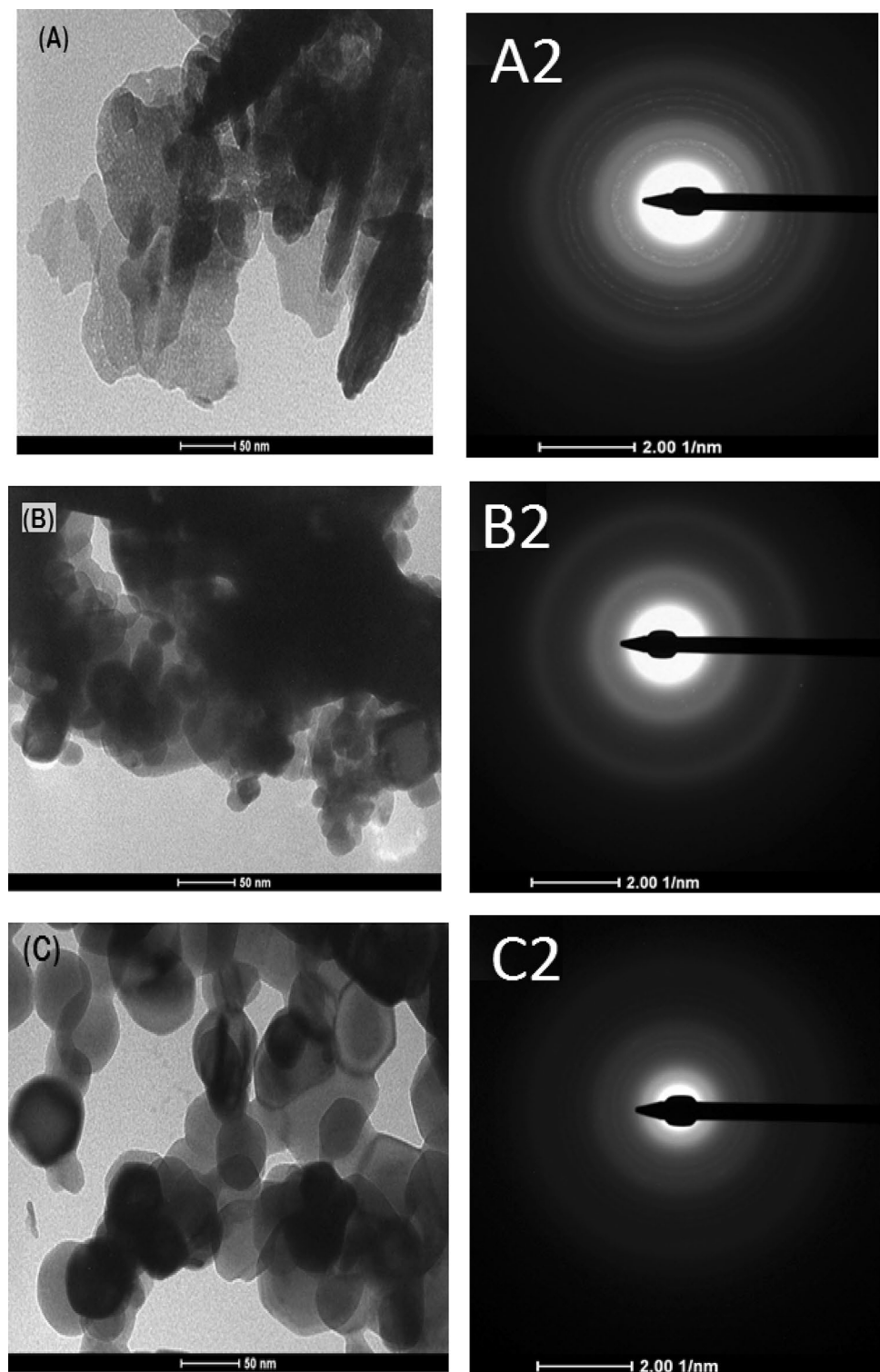
Fig. 5 SEM images of **a** ZnO nanoparticles, **b** ZnO–Ag nanocomposite, **c** ZnO–Cu nanoparticles and the EDX of (a1) ZnO nanoparticles (b1) ZnO–Ag nanocomposite (c1) ZnO–Cu nanocomposites



of the metrics. The introduction of Cu impurities to form ZnO–Cu nanocomposite, changed the nanorods and the flakes in ZnO to a spherical shape as shown in Fig. 6c. The close link between Ag and ZnO makes a strong electronic interaction that will improve the charge separation [55], this accounts for its low energy band gap when compared with ZnO–Cu nanocomposite. The average particle sizes of ZnO, ZnO–Ag and ZnO–Cu which are

< 50 nm are in consonance with XRD results. The selected area SAED pattern in Fig. 6(a2–c2) show distinct bright centric ring with further ring in Fig. 6(a2) being partially illuminated confirming the irregular orientation of its nanocrystals unlike in Fig. 6(b2, c2) which indicated a regular orientation of nanocrystals [41].

Fig. 6 TEM Image of **a** ZnO, **b** ZnO–Ag and **c** ZnO–Cu and SEAD Image of (2a) ZnO nanoparticles, (2b) ZnO–Ag nanocomposite, (2c) ZnO–Cu nanocomposite



4 Conclusion

Nanoparticles and nanocomposites were effectively synthesized by a green method using Soxhlet extracted dye of *B. ferruginea* as a reducing and capping agent. O–H, C=O, N–H, C–O and S=O were ascertained to be the functional

groups that, were involved in the reduction and stabilizing of the nano ions. The optical studies revealed a narrowing of band gap from 3.24 to 3.13 eV as Ag^{2+} and Cu^{2+} gradually substituted the Zn^{2+} ions in the ZnO matrix. High level of crystallinity and the average crystallite size of 19.02, 18.98 and 18.90 nm was recorded for ZnO, ZnO–Ag

and ZnO–Cu respectively. SEM and TEM analysis clearly indicated the formation of flakes with nanorods for ZnO, polyhedral shape with Ag dots and spherical shape upon doping of ZnO with Ag or Cu. The elemental analysis confirmed peaks for Zn, Ag, Cu and O. The bright centric ring and other non-luminous ring of the SAED revealed an irregular orientation. These findings inferred the viability of the dye extracted from *B. ferruginea* as a reducing and capping agent capable of synthesizing nanoparticles and nanocomposites that are eco-friendly with potentials in photovoltaic, electronics and photocatalytic applications.

Compliance with ethical standard

Conflict of interest The authors declare no conflicts of interest

References

- Firdhouse MJ, Lalitha P (2015) Biosynthesis of silver nanoparticles and its applications. *Rev J Nanotechnol*. <https://doi.org/10.1155/2015/829526>
- Khana SA, Noreen F, Kanwal S, Iqbal A, Hussain G (2018) Green synthesis of ZnO and Cu-doped ZnO nanoparticles from leaf extracts of *Abutilon indicum*, *Clerodendrum infortunatum*, *Clerodendrum inerme* and investigation of their biological and photocatalytic activities. *Mater Sci Eng* 82:46–59
- Kim JB, Byun D, Je SY, Park DH, Choi WK, Choi JW, Angadi B (2008) Cu-doped ZnO-based p-n hetero-junction light emitting diode. *Semicond Sci Technol* 23(9):095004–095010
- Oscar FL, Vismaya S, Arunkumar M, Thajuddin N, Dhanasekaran D, Nithya C (2016) Algal nanoparticles: synthesis and biotechnological potentials. *World's largest Science, Technology & Medicine Publisher INTECH*, pp 157–182
- Kumar J, Shrivastava V, Thakur S (2013) Synthesis and characterization of silver doped zinc oxide nanoparticles and their antifungal activity against *Aspergillus brasiliensis* and *Candida albicans*. *Adv Sci Focus* 1:346–350
- Chen S, Zhao X, Xie H, Liu J, Duan L, Ba X, Zhao J (2012) Photoluminescence of undoped and Ce-doped SnO₂ thin films deposited by sol-gel-dip-coating method. *Appl Surf Sci* 258:3255–3259. <https://doi.org/10.1016/j.apsusc.2011.11.077>
- Vijayakumar TS, Karthikeyeni S, Vasanth S, Ganesh A, Bupesh G, Ramesh G, Manimegalai M, Subramania P (2013) Synthesis of silver-doped zinc oxide nanocomposite by pulse mode ultrasonication and its characterization studies. *J Nanosci*. <https://doi.org/10.1155/2013/785064>
- Sathyavathi R, Krishna MB, Rao SMJ, Saritha R, Rao DN (2010) Biosynthesis of silver nanoparticles using *Coriandrum sativum* leaf extract and their application in nonlinear optics. *Adv Sci Lett* 3:1–6
- Kumar S, Malodia CL (2017) Biosynthesis of zinc oxide nanoparticles using leaf extract of *Calotropis gigantea*: characterization and its evaluation on tree seedling growth in nursery stage. *Appl Nanosci* 7:501–512
- Brayner R, Ferrarri-Ilou R, Brivois N, Djediat S, Benedetti MF, Levet F (2006) Toxicological impact studies based on *Escherichia coli* bacteria in ultrafine ZnO nanoparticle colloidal medium. *Nano Lett* 6(4):866–870
- Tin S, Sakharkar KR, Lim CS, Sakharkar MK (2009) Activity of Chitosan in combination with antibiotics in *Pseudomonas aeruginosa*. *Int J Biol Sci* 5(2):153–160
- Schubert EF (2005) Doping in III-V semiconductors, Cambridge studies in semiconductor physics and microelectronic engineering, 1st edn. Cambridge University Press, Cambridge
- Zhang X, Song H, Yu L, Wang T, Ren X, Kong X, Xie Y, Wang X (2006) Surface states and its influence on luminescence in ZnS nanocrystallites. *J Lumin* 118:251–256
- Rekha K, Nirmala M, Nair MG, Anukaliani A (2010) Structure, optical, photocatalytic and antibacterial activity of zinc oxide and manganese doped zinc oxide nanoparticles. *Phys B* 405:3180–3185
- Qiao SZ, Liu J, Qing G, Lu M (2011) Synthetic chemistry of nanomaterials. In: *Modern inorganic synthetic chemistry*. Elsevier, New York, pp 479–506
- Phoohinkong W, Foophow T, Pecharapa W (2017) Synthesis and characterization of copper zinc oxide nanoparticles obtained via metathesis process. *Adv Nat Sci Nanosci Nanotechnol*. <https://doi.org/10.1088/2043-6254/aa7223>
- Fu D, Han G, Chang Y, Dong J (2012) Synthesis and properties of ZnO-graphene nano hybrid for photodegradation of organic pollutant in water. *Mater Chem Phys* 132(2012):673–681
- Wang X, Ding Y, Summers CJ, Wang ZL (2004) Large scale synthesis of 6 nm wide ZnO nanobelts. *J Phys Chem* 26:8773–8777
- Ramimoghadam D, Bagheri S, Hamid SBA (2014) Biotemplated synthesis of anatase titanium dioxide nanoparticles via lignocellulosic waste material. *Biomed Res Int*. <https://doi.org/10.1155/2014/205636>
- Sharma D, Rajput J, Kaith BS, Kaur M, Sharma S (2010) Synthesis of ZnO nanoparticles and study of their antibacterial and antifungal properties. *Thin Solid File* 519:1224–1229
- Liu W, Cui Y, Zhang L, Ren S (2009) Study on extracting natural plant dyestuff by enzyme-ultrasonic method and its dyeing ability. *J Fiber Bioeng Inf* 2(1):21–30
- Deveog O, Torganc E, Karadag R (2011) High-performance liquid chromatography of some natural dyes: analysis of plant extracts and dyed textiles. *Color Technol* 128:133–138
- Rashid MA, Gustafson KR, Cardellina JH, Boyd MR (2001) A new Podophyllojoxin derivative from *Bridelia ferruginea*. *Nat Prod Lett* 14:285–292
- Orafidiya LO, Lamikanra A, Adediji JA (1990) Coagulation of milk as an index of astringency of the bark extract of *Bridelia ferruginea* Benth. and lime juice for the formulation of a traditional gargle “Ogun Efu”. *Phytother Res* 4:189–194
- Cimanga K, De-Bruyne T, Apers S, Dieters L, Totte J, Kambu K, Tona L, Bakana P, Van-Ufford LQ, Beukelman C, Labadie R, Vlietinck AJ (1999) Complement-inhibiting constituents of *Bridelia ferruginea* stem bark. *Planta Med* 65:213–217
- Olarewaju O, Oloyede O, Ojo O, Onikanni A, Ajiboye B (2014) In-vitro antioxidant activities of the stem bark extract fractions of *Bridelia ferruginea*. *J Biol Agric Healthc* 4(3):1–7
- Yedurkar S, Maurya C, Mahanwar P (2016) Biosynthesis of zinc oxide nanoparticles using *Ixora coccinea* leaf extract—a green approach. *Open J Synth Theory Appl* 5:1–14. <https://doi.org/10.4236/ojsta.2016.51001Y>
- Mohammed MA, Abu-Taleb A, Remalli N, Abdullah M, Srikanth Vadali SVSS, Labhasetwa NK (2013) Dragon's blood aided synthesis of Ag/Ag₂O core/shell nanostructures and Ag/Ag₂O decorated multi-layered graphene for efficient As(III) uptake from water and antibacterial activity. *RSC Adv*. <https://doi.org/10.1039/c6ra05061aa>
- Ahmad A, Li B, Khan AU, Shah SAA, Khan GM, Khan ZUH, Khan Q, Khan FU (2016) Biodirected Synthesis of Palladium nanoparticles using *Phoenix dactylifera* leaves extract and their size

- dependent biomedical and catalytic applications. RSC Adv. <https://doi.org/10.1039/c6ra11409a>
30. Hong H, Chen HB, Yang DH, Shang MY, Wang X, Cai SQ, Mikage M (2011) Comparison of content of five ephedrine alkaloids in three official origin of Ephedra Herb in China by high-performance liquid chromatography. J Nat Med 65:623–628. <https://doi.org/10.1007/s11418-011-0528-8>
 31. Gul R, Jan SU, Farklullah S, Sherani S, Jahan N (2017) Preliminary phytochemical screening, quantitative analysis of alkaloid and antioxidant activity of crude plant extracts from Ephedra Intermedia Indigenous to Balochistan. Sci Word J. <https://doi.org/10.1155/2017/5873648>
 32. Jamous R, Zaitoun S, Husein A, Qasem I, Ali-Shtayeh M (2015) Screening for biology activities of medicinal plants used in traditional Arabic Palestinian herbal medicine. Eur J Med plant 9:1–13
 33. Karande AM, Kamble HV, Kumbhar VH, Kane SR, Magdum CS (2016) Preliminary phytochemical screening of *Glochidion ellipticum*. Eur J Exp Biol 6(4):41–45
 34. Ezeonu SC, Ejikeme CM (2016) Qualitative and quantitative determination of phytochemical contents of indigenous Nigerian softwoods. New J Sci. <https://doi.org/10.1155/2015/>
 35. Vanaja M, Annadurai G (2013) Coleus aromaticus leaf extract mediated synthesis of silver nanoparticles and its bactericidal activity Applied. Nanoscience 3:217–223. <https://doi.org/10.1007/s13204-012-0121-9>
 36. Mphande BC, Pogrebnoi A (2014) Impact of extraction methods upon light absorbance of natural organic dyes for dye sensitized solar cells application. J Energy Nat Res 3(3):38–45
 37. Lattanzio V, Lattanzio VMT, Cardinali A (2006) Role of phenolics in the resistance mechanisms of plants against fungal pathogens and insects. In: Imperato F (ed) Phytochemistry: advances in research. Research Signpost, Thiruvananthapuram, pp 23–67
 38. Selim KA, Khalil KE, Abdel-Bary MS, Abdel-Azeim NA (2008) Extraction, Encapsulation and utilization of red pigments from roselle (*Hibiscus sabdariffa* L.) as natural food colourants. Special Volume Conference, Alex J Food Sci Technol 7–20
 39. Prasad R, Swamy VS (2013) Antibacterial activity of silver nanoparticles synthesized by Bark Extract of *Syzygium cumini*. J Nanopart. <https://doi.org/10.1155/2013/431218>
 40. Awwad AN, Salem NM, Abdeen AO (2013) Green synthesis of silver nanoparticles using carob leaf extract and its antibacterial activity. Int J Ind Chem 4(1):29. <https://doi.org/10.1186/2228-5547-4-29>
 41. Talam S, Karumuri SR, Gunnam N (2012) Synthesis, characterization, and spectroscopic properties of ZnO nanoparticles. Nanotechnology. <https://doi.org/10.5402/2012/372505>
 42. Varadavenkatesan T, Lyubchik E, Pai S, Pugazhendhi A, Vinayagam R, Selvaraj R (2019) Photocatalytic degradation of Rhodamine B by zinc oxide nanoparticles synthesized using the leaf extract of *Cyanometra ramiflora*. J Photochem Photobiol B Photobiol B Biol 199:111621
 43. Shraddha P, Sridevi H, Thivaharan V, Ramesh V, Raja S (2019) Photocatalytic zinc oxide nanoparticles synthesis using *Peltophorum pterocarpum* leaf extract and their characterization. Optik Int J Light Electron Optics 185:248–255. <https://doi.org/10.1016/j.ijleo.2019.03.101>
 44. Kumar B, Smita K, Cumbal L, Debut A (2017) Green synthesis of silver nanoparticles using Andean blackberry fruit extract. Saudi J Biol Sci 24(1):45–50. <https://doi.org/10.1016/j.sjbs.2015.09.006>
 45. Omotunde OI, Okoronkwo AE, Aiyesanm AF, Gurgur E (2018) Photocatalytic behavior of mixed oxide NiO/PdO nanoparticles toward degradation of methyl red in water. J Photochem Photobiol A 365:145–150
 46. Yusof AS, Hassan Z (2018) Fabrication and characterization of Cu-doped ZnO films using RF reactive magnetron sputtering. J Phys. <https://doi.org/10.1088/1742-6596/1083/1/012062>
 47. Lim SP, Pandikumar A, Lim HN, Ramaraj R, Huang NM (2015) Boosting photovoltaic performance of dyesensitized solar cells using silver nanoparticle-decorated N, S-Co-doped-TiO₂ photoanode. Sci Rep 5:11922. <https://doi.org/10.1038/srep11922>
 48. Ghosh A, Kumari N, Bhattacharjee A (2015) Influence of Cu doping on structural, electrical and optical properties of ZnO. Pramana 84(4):621–635
 49. Zhou J, Zhao F, Wang Y, Zhang Y, Yang L (2007) Size controlled synthesis of ZnO nanoparticles and their photoluminescence properties. J Lumin 122–123(1–2):195–197
 50. Khoshshesab Z, Sarfaraz M, Asadabad MA (2011) Preparation of ZnO nanostructures by chemical precipitation method. Synth React Inorg Met Org Chem 41:814–819
 51. JCPDS, Powder Diffraction File, Alphabetical Index, Inorganic Compounds, International Centre for Diffraction Data, Newtown Square, Pa, USA (1977)
 52. Dinesha VP, Bija P, Ashoka A, Dharab SK, Kamaruddinb M, Tyagib AK, Raja B (2014) Plasmon-mediated highly enhanced photocatalytic degradation of industrial textile effluent dyes using hybrid ZnO@Ag Core-shell Nanorods. RSC Adv 4:58930–58940. <https://doi.org/10.1039/C4RA09405K>
 53. Singh R, Barman PB, Sharma D (2017) Synthesis, structural and optical properties of Ag doped ZnO nanoparticles with enhanced photocatalytic properties by photo degradation of organic dyes. J Mater Sci Mater Electron 28:5705–5717
 54. Mukhtar M, Munisa L, Saleh R (2012) Co-precipitation of synthesis and characterization of nanocrystalline zinc oxide particles dope with Cu²⁺ ions. Mater Sci Appl 3(8):543–551. <https://doi.org/10.4236/msa.2012.3807>
 55. Mashwani Z, Khan MA, Khan T, Nadhman A (2016) Applications of plant terpenoids in the synthesis of colloidal silver nanoparticles. Adv Colloid interface Sci 234:134–141. <https://doi.org/10.1016/j.cis.2016.04.008>

Publisher's Note Springer Nature remains neutral with regard to jurisdictional claims in published maps and institutional affiliations.